Inorg. Chem. **2004**, *43*, 6762–6773

Fine Tuning of the Electronic Coupling between Metal Centers in Cyano-Bridged Mixed-Valent Trinuclear Complexes

Pablo Alborés,[†] Leonardo D. Slep,[†] Thomas Weyhermüller,[‡] and Luis M. Baraldo*[,†]

Departamento de Química Inorgánica, Analítica y Química Física, INQUIMAE, Facultad de Ciencias Exactas y Naturales, Universidad de Buenos Aires, Pabellón 2, Ciudad Universitaria, C1428EHA Buenos Aires, Argentina, and Max-Planck-Institut für Bioanorganische Chemie, Stiftstrasse 34-36, D-45470 Mülheim an der Ruhr, Germany

Received May 16, 2004

We report the synthesis, characterization, and spectroscopic properties of a family of trinuclear cyano-bridged mixed-valent compounds, *trans*-$[Ru^{II}L_4\{NCFe^{III}(CN)_5\}_2]^{4-}$, *trans*-$[Ru^{II}L_4\{CNFe^{III}(CN)_5\}_2]^{4-}$, and *cis*-$[Ru^{II}(bpy)_2\{NCFe^{III}(CN)_5\}_2]^{4-}$ (L = pyridine, 4-*tert*-butylpyridine, and 4-methoxypyridine). Tetraphenylphosphonium salts of complexes *trans*-$[Ru^{II}L_4\{NCFe^{III}(CN)_5\}_2]^{4-}$ (L = pyridine and 4-*tert*-butylpyridine) crystallize in the space groups *C*2 and $P2_1/c$, respectively, and show a linear arrangement of the metal units and an almost completely eclipsed configuration of the equatorial ligands. An intense band ($\epsilon \sim$ 2000–9000 M^{-1} cm^{-1}) is observed for all of the compounds in the NIR region of the spectrum, not present in the separated building blocks, and strongly solvent dependent. We assign it as a metal-to-metal charge transfer (MMCT) from the Ru(II) to the terminal Fe(III) moieties in the context of a simplified three-center model. The electrochemistry measurements reveal a splitting of the redox waves for the reduction of the iron centers for some of the complexes with a trans configuration between the metal units, ranging from 100 to 260 mV, depending on the substituting pyridine ligand and the solvent, suggesting long-range metal–metal interactions. These interactions are rationalized in terms of the energy matching between the π-symmetry orbitals of the metals and the cyanide bridge. The one- and two-electron reduced species derived from compounds *trans*-$[Ru^{II}L_4\{NCFe^{III}(CN)_5\}_2]^{4-,5-,6-}$ were characterized in methanolic solution. The mixed-valent Fe^{II}–Ru^{II}–Fe^{III} system exhibits an intense red shifted band in the NIR region of the spectrum, arising from the superposition of MMCT bands from the central Ru(II) to the terminal Fe(III) fragments and from the 1 nm distant Fe(II) to Fe(III) centers.

Introduction

In recent years, the exploration of the properties of cyanide-bridged systems has uncovered several M−CN−M′ assemblies with moderate to strong metal−metal interactions and interesting magnetic, photophysical, and electronic properties.[1] The systems containing terminal cyanides are particularly attractive because of the possibility for using them in the construction of larger and more complex arrays.[2] Among the possible combinations, those leading to linear assemblies stand probably as the more attractive targets. Their symmetry makes them ideal for studying long-range electron-transfer processes leading eventually to molecular wires.[3] They also provide maximum charge separation in photophysical processes, making them attractive in the construction of light-harvesting devices.[4]

Unfortunately, most of the published attempts to build large cyanide-bridge clusters lead to insoluble or unfusible materials that are difficult or impossible to process. The lack of success is probably related to the commonly used synthetic

* Author to whom correspondence should be addressed. E-mail: baraldo@qi.fcen.uba.ar.
[†] Universidad de Buenos Aires.
[‡] Max-Planck-Institut für Bioanorganische Chemie.

(1) (a) Mallah, T.; Thiébaut, S.; Verdaguer, M.; Veillet, P. *Science* **1993**, *262*, 1554. (b) Entley, W. R.; Girolami, G. S. *Science* **1995**, *268*, 397−400. (c) Heintz, R. A.; Dunbar, K. R. *Prog. Inorg. Chem.* **1997**, *45*, 283.
(2) Bignozzi, C. A.; Argazzi, R.; Bortolini, O.; Scandola, F.; Harriman, A. *New J. Chem.* **1996**, *20*, 731−738.
(3) Launay, J.-P.; Coudret, C. Wires Based on Metal Complexes. In *Electron Transfer in Chemistry*; Balzani, V., Ed.; Wiley-VCH: Weinheim, Germany, 2001; Vol. 5, Chapter 1.
(4) (a) Balzani, V.; Juris, A.; Venturi, M.; Campagna, S.; Serroni, S. *Chem. Rev.* **1996**, *96*, 759. (b) Bignozzi, C. A.; Schoonover, J. R.; Scandola, F. *Prog. Inorg. Chem.* **1997**, *44*, 1. (c) Balzani, V.; Campagna, S.; Denti, G.; Juris, A.; Serroni, S.; Venturi, M. *Acc. Chem. Res.* **1998**, *31*, 26.

10.1021/ic0493649 CCC: $27.50
Published on Web 09/22/2004

Scheme 1. Anions Reported in This Work

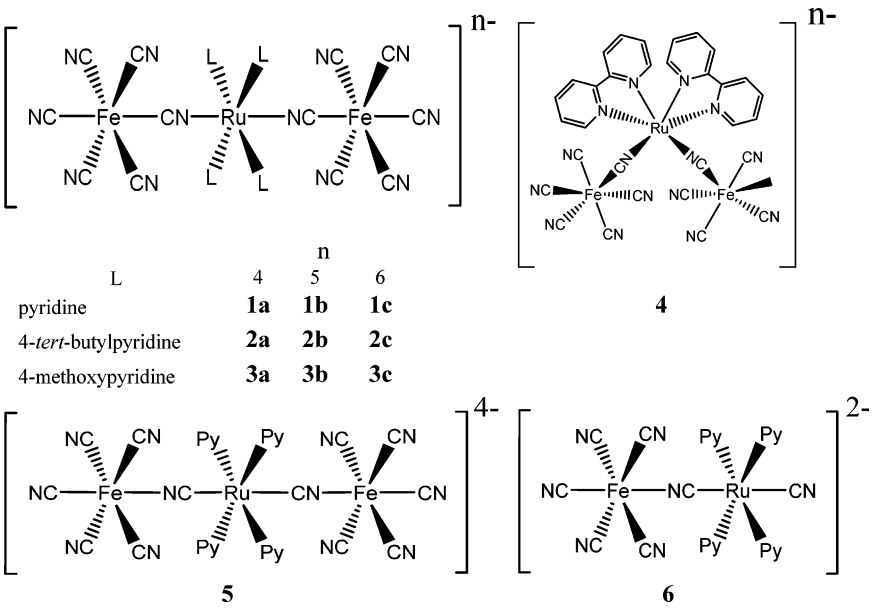

L	n = 4	5	6
pyridine	**1a**	**1b**	**1c**
4-*tert*-butylpyridine	**2a**	**2b**	**2c**
4-methoxypyridine	**3a**	**3b**	**3c**

4 **5** **6**

strategy. Typically, mononuclear cyanide-containing complexes are condensed with labile species (generally some transition-metal hexaaquo-metalate species) in a normally kinetically difficult to control process. An alternative to this procedure would involve the controlled concatenation of preformed small soluble oligonuclear fragments with molecular characteristics that constrain the topology of the resulting cluster. In this direction, we are exploring the potential use of linear trinuclear species holding terminal cyanides. Surprisingly, only a few soluble oligomers have been reported,[5] and structural determinations of the arrangements of at least three metal atoms are still scarce.[5,6] *trans*-$[(NH_3)_4Pt^{IV}\{NC-Fe^{II}(CN)_5\}_2]^{4-}$ stands as the sole example of a structurally characterized linear trinuclear compound containing terminal cyanides and, for that reason, is suitable for the construction of larger units.[7]

In this work, we report the synthesis and the structural, electrochemical, and spectroscopic characterization of a family of trinuclear compounds, $[Ru^{II}L_4\{NCFe^{III}(CN)_5\}_2]^{4-}$ and $[Ru^{II}L_4\{CNFe^{III}(CN)_5\}_2]^{4-}$ (Scheme 1), bearing terminal cyanides and intramolecular cyanide bridges, where the interaction between the metals can be tuned by varying the basicity of the L ligands, the orientation of the cyanide bridge, the configuration around the ruthenium ion, or the interaction of the terminal cyanides with the solvent.

Experimental Section

Materials. Complexes *trans*-$Ru(CN)_2(py)_4$, *trans*-$RuCl_2(py)_4$, *trans*-$RuCl_2(dmso)_4$, *cis*-$Ru(bpy)_2Cl_2\cdot 2H_2O$, and $Na_2[Fe(CN)_5NH_3]\cdot 2H_2O$ were prepared according to previously published procedures.[8,9] Solvents for UV−visible and electrochemistry measurements were dried according to literature procedures.[10] The tetra-*n*-butylammonium hexafluorophosphate ($TBAPF_6$) used in the cyclic voltammetry experiments was recrystallized from ethanol. All other reagents were obtained commercially and used as supplied. The compounds synthesized in this work were routinely dried in a vacuum desiccator for at least 12 h prior to characterization.

Synthesis of the Complexes. *trans*-$[L_4Ru^{II}\{NC-Fe^{III}(CN)_5\}_2][Ph_4P]_4$ [L = pyridine (1a), 4-*tert*-butylpyridine (2a), and 4-methoxypyridine (3a)]. In a typical preparation, 2 mmol of $[RuL_4Cl_2]$[11] and a large excess of $K_3[Fe(CN)_6]$ (40 mmol) were suspended in 50 mL of a 4:1 mixture of water and methanol. The reaction mixture was heated to reflux for 4 h and protected from sunlight. Along the course of the reaction, the ruthenium precursor dissolves completely, yielding a deep-green solution. When the solution was cooled to room temperature, the excess of $K_3[Fe(CN)_6]$ was precipitated by the addition of ∼100 mL of methanol. The yellowish solid was removed by filtration and washed thoroughly with methanol. The combined filtrates were concentrated up to a few milliliters and treated with an excess of tetraphenylphosphonium chloride. After the solution was left to stand overnight at −18 °C, the crude product was collected by filtration as a green solid, washed with water, and vacuum-dried.

Purification was performed by exclusion chromatography using a Sephadex LH-20 column (l = 60 cm, ϕ = 4 cm) packed and eluted with methanol. The second colored fraction that eluted from the column was collected and evaporated to dryness, and the green solid was dried under vacuum. Further purification was achieved by

(5) (a) Vahrenkamp, H.; Geiss, A.; Richardson, G. N. *J. Chem. Soc., Dalton Trans.* **1997**, 3643−3651. (b) Zhu, N. Y.; Vahrenkamp, H. *J. Organomet. Chem.* **1999**, *573*, 67−72. (c) Richardson, G. N.; Brand, U.; Vahrenkamp, H. *Inorg. Chem.* **1999**, *38*, 3070−3079. (d) Geiss, A.; Vahrenkamp, H. *Inorg. Chem.* **2000**, *39*, 4029−4036. (e) Chen, Z. N.; Appelt, R.; Vahrenkamp, H. *Inorg. Chim. Acta* **2000**, *309*, 65−71. (f) Richardson, G. N.; Vahrenkamp, H. *J. Organomet. Chem.* **2000**, *594*, 44−48. (g) Appelt, R.; Vahrenkamp, H. *Z. Anorg. Allg. Chem.* **2003**, *629*, 133−138.

(6) Sheng, T. L.; Vahrenkamp, H. *Eur. J. Inorg. Chem.* **2004**, 1198−1203.

(7) Zhou, M. S.; Pfennig, B. W.; Steiger, J.; Vanengen, D.; Bocarsly, A. B. *Inorg. Chem.* **1990**, *29*, 2456−2460.

(8) (a) Kenney, D. J.; Flynn, T. P.; Gallini, J. B. *J. Inorg. Nucl. Chem.* **1961**, *20*, 75. (b) Evans, I. P.; Spencer, A.; Wilkinson, G. *J. Chem. Soc., Dalton Trans.* **1973**, 204−209. (c) Sullivan, B. P.; Salmon, D. J.; Meyer, T. J. *Inorg. Chem.* **1978**, *17*, 3334−3341.

(9) Coe, B. J.; Meyer, T. J.; White, P. S. *Inorg. Chem.* **1995**, *34*, 593−602.

(10) Armarego, W. L. F.; Perrin, D. D. *Purification of Laboratory Chemicals*, 4th ed.; Butterworth-Heinemann: Oxford, 1996.

(11) Complexes RuL_4Cl_2, with L = 4-*tert*-butylpyridine and 4-methoxypyridine, were prepared in the following manner. $Ru(dmso)_4Cl_2$ (2 mmol) was suspended in 25 mL of absolute ethanol, and 80 mmol of the ligand was added. After the solution was refluxed and stirred for about 3 h, the orange microcrystalline solid obtained was collected by filtration, washed with ethanol, and dried in vacuum. Yield: 60−70%. These materials were used without further purification.

recrystallization from methanol/ether. Yields ranged between 30 and 60% depending on the pyridinic precursor. Anal. Calcd for (**1a**·$9H_2O$) $C_{128}H_{118}N_{16}O_9P_4Fe_2Ru$: C, 65.1; H, 5.0; N, 9.5. Found: C, 64.9; H, 4.8; N, 9.2. IR (CN) ν: 2107 (s) cm^{-1}. Anal. Calcd for (**2a**·$7H_2O$) $C_{144}H_{146}N_{16}O_7P_4Fe_2Ru$: C, 67.8; H, 5.7; N, 8.8. Found: C, 67.8; H, 5.5; N, 8.7. IR (CN) ν: 2106 (s) cm^{-1}. Anal. Calcd for (**3a**·$10H_2O$) $C_{132}H_{128}N_{16}O_{10}P_4Fe_2Ru$: C, 63.4; H, 5.1; N, 9.0. Found: C, 63.8; H, 5.1; N, 9.1. IR (CN) ν: 2108 (s) cm^{-1}.

***cis*-[(bpy)$_2$Ru^{II}{(μ-NC)Fe^{III}(CN)$_5$}$_2$](Ph$_4$P)$_4$ (4).** A suspension of 0.15 g of *cis*-Ru(bpy)$_2$Cl$_2$·$2H_2O$ (0.29 mmol) and 1.9 g of K_3[Fe(CN)$_6$] (5.8 mmol) in 50 mL of a water/methanol (1:1) mixture was heated to reflux and protected from sunlight for 2 h. After the mixture was cooled to room temperature, ~100 mL of methanol was added to precipitate the excess of hexacyanoferrate(III). The solid was removed by filtration, and the clear solution evaporated until only a few milliliters of water remained. Addition of 1.00 g of tetraphenylphosphonium chloride afforded an oily suspension, which when left to stand overnight at −18 °C, turned into a fine precipitate. The solution was decanted and the solid dried under vacuum. The dark-red hygroscopic material was dissolved in the minimum amount of methanol and purified twice through a Sephadex LH-20 column (l = 60 cm, ϕ = 4 cm) packed and eluted with methanol. The product eluted as the third colored fraction. The latter was collected, evaporated to dryness, and further dried under vacuum, yielding 0.1 g of **4** (14%). Anal. Calcd for (**4**·$12H_2O$) $C_{128}H_{120}N_{16}O_{12}P_4Fe_2Ru$: C, 63.8; H, 5.0; N, 9.3. Found: C, 63.6; H, 5.1; N, 9.4. IR (CN) ν: 2107 (s) cm^{-1}.

***trans*-[py$_4$Ru^{II}{(μ-CN)Fe^{III}(CN)$_5$}$_2$](Ph$_4$P)$_4$ (5) and *trans*-[NCRu^{II}py$_4$(μ-CN)Fe^{III}(CN)$_5$](Ph$_4$P)$_2$ (6).** In a typical preparation, a solution of 0.30 g of Ru(py)$_4$(CN)$_2$ (0.64 mmol) and 0.274 g of Na_2[Fe(CN)$_5$(NH_3)]·$2H_2O$ (0.96 mmol) in 10 mL of a water/methanol (1:1) mixture was stirred at room temperature for 24 h, yielding a deep-green solution. The mixture was evaporated to dryness in a rotary evaporator, and the solid residue was redissolved in the minimum amount of water and filtered to remove some insoluble material, probably Prussian blue-like polymeric compounds. The clear solution was treated with solid tetraphenylphosphonium chloride to afford a light-blue precipitate. The solid material was collected by filtration, washed thoroughly with water, and dried to yield 0.47 g of crude product, which proved to be a mixture of the trinuclear **5** and dinuclear **6** species. The mixture was resolved by repetitive (two to three times) exclusion chromatography on a Sephadex LH-20 column (l = 60 cm, ϕ = 4 cm) packed and eluted with methanol. The larger anion **5** eluted first, while the smaller **6** was retained longer in the column. These two fractions were collected and evaporated to dryness. The purification process yielded 320 mg of pure **5** (yield = 22% based on Ru) and a much smaller amount (31 mg, 3% based on Ru) of **6**. Anal. Calcd for (**5**·$2H_2O$) $C_{128}H_{104}N_{16}O_2P_4Fe_2Ru$: C, 68.8; H, 4.7; N, 10.0. Found: C, 69.0; H, 4.7; N, 10.0. IR (CN) ν: 2111 (s), 2088 (s) cm^{-1}. Anal. Calcd for (**6**·$6H_2O$) $C_{75}H_{72}N_{11}O_6P_2FeRu$: C, 62.5; H, 5.0; N, 10.7. Found: C, 62.7; H, 4.8; N, 10.0. IR (CN) ν: 2109 (s), 2063 (s) cm^{-1}.

Sodium salts of the reported new complexes were prepared in a water solution in the following way. The tetraphenylphosphonium derivatives were dissolved in the minimum amount of acetonitrile and treated with solid $NaClO_4$. The sodium salts precipitated immediately and were collected by filtration, washed with acetonitrile, and vacuum-dried. These solids were redissolved in water and filtered again to yield the aqueous solutions employed in the spectroscopic measurements.

Physical Measurements. IR spectra were collected with a Nicolet FTIR 510P instrument on KBr pellets. UV−visible spectra were recorded with a Hewlett-Packard 8453 diode array spectrometer in the range between 190 and 1100 nm or with a Shimadzu 3100 UV−vis−NIR for the NIR (up to 3000 nm) region. Elemental analyses were performed with a Carlo Erba 1108 analyzer. Cyclic voltammetry measurements were carried out under argon with millimolar solutions of the compounds using a PAR 273A potentiostat and a standard three-electrode arrangement consisting of a glassy carbon disk (area = 9.4 mm^2) as the working electrode, a platinum wire as the counter electrode, and a reference electrode. Depending on the situation, the latter was either a Ag/AgCl 3 M KCl standard electrode (for aqueous solutions) or a silver wire with an internal ferrocene (Fc) standard for organic solvents. KNO_3 (1 M) and tetra-*n*-butylammonium hexafluorophosphate ($TBAPF_6$) (0.1 M) were used as the supporting electrolytes in water and nonaqueous media, respectively. All of the potentials reported in this work are referenced to the standard Ag/AgCl 3 M KCl electrode (0.21 V vs NHE), with the conversions being performed by using the accepted values for the Fc^+/Fc couple in different media.[12]

Table 1. Crystal Data Collection for Complexes **1a** and **2a**

	1a	**2a**
empirical formula	$C_{144}H_{168}Fe_2N_{16}O_{18}P_4Ru$	$C_{152}H_{170}Fe_2N_{16}O_{11}P_4Ru$
fw	2747.59	2733.69
T (K)	100(2)	100(2)
wavelength (Å)	0.71073	0.71073
cryst syst	monoclinic	monoclinic
space group	$C2$	$P2_1/c$
lattice params		
a (Å)	24.275(2)	15.631(1)
b (Å)	23.162(2)	14.562(1)
c (Å)	14.6189(9)	32.643(3)
β (deg)	102.96(2)	91.24(1)
vol (Å^3)	8010.2(11)	7428.4(10)
Z	2	2
density$_{calcd}$ (mg/m^3)	1.139	1.222
abs coeff (mm^{-1})	0.373	0.398
final indices (R1)	0.0833	0.0732
$I > 2\sigma(I)$ (wR2)	0.2123	0.1789
indices (R1)	0.1137	0.1031
all data (wR2)	0.2472	0.2021

X-ray Crystallographic Data Collection and Refinement of the Structures. Single green crystals of **1a** and **2a** were coated with perfluoropolyether, picked up with a glass fiber, and immediately mounted in the cold nitrogen stream of the diffractometer to prevent the loss of solvent. Intensity data were collected at 100 K using a Nonius Kappa CCD diffractometer equipped with a Mo target rotating anode X-ray source and a graphite monochromator (Mo Kα, λ = 0.71073 Å). Final cell constants were obtained from a least-squares fit of a subset of several thousand strong reflections. Data collection was performed by taking frames at a 1.0° rotation in ω, covering more than half of the diffraction sphere. Crystal faces were determined, and the corresponding intensity data were corrected for absorption using the Gaussian-type routine embedded in XPREP.[13] Crystallographic data of the compounds are listed in Table 1. The Siemens SHELXTL-PLUS[13] software package was used for the solution and artwork of the structures. SHELXL97[14] was used for the structure refinement. The structures were readily solved by direct methods and subsequent difference Fourier techniques. The structure of **1a** was refined in space group $C2$ (No. 5), but the crystal appeared to be racemically twined. All nonhydrogen atoms of the complex anion and the phosphonium cations

(12) Noviandri, I.; Brown, K. N.; Fleming, D. S.; Gulyas, P. T.; Lay, P. A.; Masters, A. F.; Phillips, L. *J. Phys. Chem. B* **1999**, *103*, 6713−6722.

(13) *SHELXTL*, version 5; Siemens Analytical X-Ray Instruments, Inc.: Madison, WI, 1994.

were refined anisotropically, and hydrogen atoms were placed at calculated positions and refined as riding atoms with isotropic displacement parameters. The solvent molecules were found to be disordered and poorly defined and were therefore isotropically refined. The C−O bond distances of the methanol molecules were restrained to be equal (within error) using the SADI instructions of SHELXL.

The *tert*-butylpyridine ligands and solvent molecules in compound **2a** were found to be disordered. Two split positions with equal occupation factors were refined for the *tert*-butyl groups of the pyridine ligands. The C−C bond distances were restrained to be equal (within certain errors), and the corresponding C atoms were isotropically refined. Some of the methanol solvent molecules were disordered and poorly defined and were therefore isotropically refined. The methanol and water positions, O(600)/O(610) and O(700)/O(710), were found to mix up and were refined with equal occupancies.

Electronic Spectroscopy of 1b−3b and 1c−3c. Spectra for the reduced species derived from some of the compounds presented in this work were obtained by chemical reduction using a previously titrated solution of $Na_2S_2O_4$ in methanol and 0.1 M 18-crown-6 (see Results for a detailed description of the mathematical methodology used to obtain the spectra of these species). All of the manipulations used to prepare the solutions were performed inside an argon-filled glovebox. The samples were then transferred to a gastight UV−vis cuvette and removed from the box to collect the spectra.

Results

Synthesis. The reaction between *trans*-RuL_4Cl_2 (L = pyridine, 4-*tert*-butylpyridine, or 4-methoxypyridine) and a large excess of potassium hexacyanoferrate(III), refluxing in a water/methanol (4:1) solution, yielded intensely green-colored solutions. The unreacted $[Fe(CN)_6]^{3-}$ could be easily removed from the reaction mixture by the addition of methanol. Metathesis of K^+ by PPh_4^+, followed by size exclusion chromatography on Sephadex LH-20, led to deep-green materials, which on the basis of all of the available analytical evidence are best formulated as *trans*-$[L_4Ru^{II}\{NC-Fe^{III}(CN)_5\}_2][Ph_4P]_4$ (compounds **1a**−**3a**). A similar procedure using *cis*-$Ru(bpy)_2Cl_2\cdot 2H_2O$ as the starting material yielded the hygroscopic dark-red *cis*-$[(bpy)_2Ru^{II}\{(\mu\text{-NC})\text{-}Fe^{III}(CN)_5\}_2](Ph_4P)_4$ (compound **4**).

Green solutions were also obtained when the substitutionally inert *trans*-$RuL_4(CN)_2$ was allowed to react at room temperature with $[Fe(CN)_5(NH_3)]^{2-}$ for periods as long as 24 h. When a delicate purification procedure mainly based on exclusion chromatography was performed, *trans*-$[py_4Ru^{II}\{(\mu\text{-CN})Fe^{III}(CN)_5\}_2](Ph_4P)_4$ (**5**) was isolated as the main product. One byproduct of the reaction proved to be the heterodinuclear *trans*-$[NCRu^{II}py_4(\mu\text{-CN})Fe^{III}(CN)_5]^{2-}$, which despite the poor yield could be isolated as a PPh_4^+ salt (compound **6**).

X-ray quality single crystals of the PPh_4^+ salts of **1a** and **2a** were obtained by the slow diffusion of ethyl ether over methanolic solutions of the compounds. The crystalline material obtained in this way showed a marked tendency to lose solvent molecules but still rendered good-quality X-ray diffraction patterns.

Table 2. Selected Bond Lengths (Å) and Angles (deg) for **2a**

N(10)−Ru(1)	2.016(4)	N(13)−C(13)	1.123(8)
C(10)−Fe(1)	1.922(5)	N(14)−C(14)	1.127(7)
N(10)−C(10)	1.139(6)	N(15)−C(15)	1.112(8)
N(11)−C(11)	1.154(6)	N(40)−Ru(1)	2.106(5)
N(12)−C(12)	1.121(9)	N(30)−Ru(1)	2.059(7)
N(10)−C(10)−Fe(1)	176.3(6)	C(10)−Fe(1)−C(13)	90.8(3)
C(10)−N(10)−Ru(1)	177.9(5)	C(10)−Fe(1)−C(12)	86.4(3)
N(11)−C(11)−Fe(1)	178.5(5)	N(10)−Ru(1)−N(40)	89.6(2)
C(10)−Fe(1)−C(15)	87.7(2)	N(10)−Ru(1)−N(30)	88.9(2)
C(10)−Fe(1)−C(14)	91.2(2)		

Crystal Structure Determinations. The crystal structures of **1a** and **2a** were determined by X-ray crystallography. Tables 2 and 3 summarize selected bond distances and angles. Figure 1 shows the structures of the anions in the crystals of the above-mentioned compounds.

Both compounds display a roughly linear trinuclear CN-bridged arrangement of the metal centers, with Fe−C−N (bridge) angles of 176.2 and 175.6° and Ru−N−C (bridge) angles of 177.9 and 174.3° for **1a** and **2a**, respectively. The Fe−Ru bond distances in both compounds are not significantly different (5.075 and 5.086 Å for **1a** and **2a**, respectively), leaving the terminal metal centers more than 1 nm apart.

The coordination environment around the terminal Fe atoms is essentially octahedral, with comparable average Fe−C and C−N bond distances for both compounds (1.956 and 1.129 Å for **1a** and 1.949 and 1.146 Å for **2a**), which do not differ significantly from the values measured in the parent hexacyanoferrate(III) ion (1.945 and 1.156 Å for the Fe−C and C−N bonds in the PPh_4^+ derivative).[15]

The conformation of the equatorial ligands around the Ru centers in **1a** preserves the usual propeller-like configuration observed for other tetrakispyridine compounds,[9,16] with an average Ru−N bond distance of 2.083 Å and a mean tilting angle of 26.9°, comparable to previous reports in other Ru-$(py)_4L_2$ species.[9] The Ru center lies in an axially compressed N_6 environment, with a Ru−N(nitrile) bond distance of 2.017 Å, which is considerably shorter than that of the Ru−N(py) bond. The situation is somewhat different in **2a**, where the *tert*-butylpyridine ligands adopt an unusual configuration with alternating orientations of the aromatic rings. Apart from that, the Ru−N(py) and Ru−N(nitrile) bond distances and the mean tilting angle (25.3°) are similar to the ones observed in the pyridine derivative.

The most remarkable structural feature of **1a** and **2a** is that all of the equatorial ligands on the three metal centers adopt an almost perfectly eclipsed conformation (Figure 1), instead of the sterically less-demanding staggered one observed in the closely related trinuclear species *trans*-$[(NH3)_4Pt^{IV}\{NC-Fe^{II}(CN)_5\}_2]^{4-}$ ion.[7]

Electrochemistry. All of the compounds reported in this work are soluble in a wide range of solvents without apparent

(14) Sheldrick, G. M. *SHELXL97*; University of Göttingen, Göttingen, Germany, 1997.

(15) Dean, P. A. W.; Fisher, K.; Craig, D.; Jennings, M.; Ohene-Fianko, O.; Scudder, M.; Willett, G.; Dance, I. *Dalton Trans.* **2003**, 1520−1528.

(16) Coe, B. J.; Meyer, T. J.; White, P. S. *Inorg. Chem.* **1995**, *34*, 3600−3609.

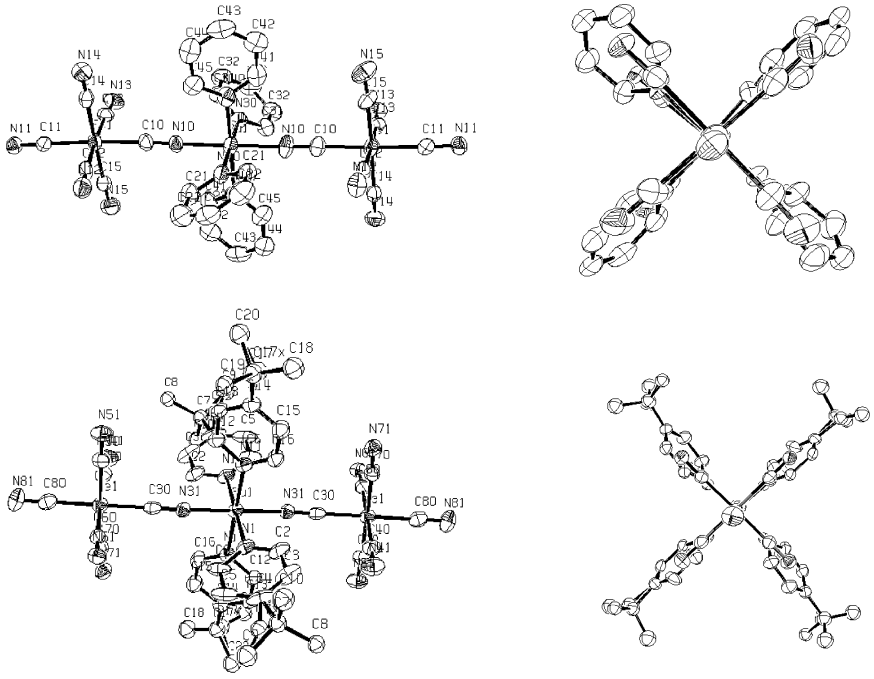

Figure 1. Structural representation (left) of anions **1a** (top) and **2a** (bottom). View along the NC−Fe−CN−Ru−NC−Fe−CN axis (right) for **1a** (top) and **2a** (bottom).

Table 3. Selected Bond Lengths (Å) and Angles (deg) for **1a**

N(31)−Ru(1)	2.011(5)	N(81)−C(80)	1.148(8)
C(30)−Fe(1)	1.944(7)	N(51)−C(50)	1.144(7)
N(31)−C(30)	1.146(7)	N(71)−C(70)	1.145(7)
N(41)−C(40)	1.144(8)	N(1)−Ru(1)	2.098(5)
N(61)−C(60)	1.144(7)	N(11)−Ru(1)	2.102(5)
N(31)−C(30)−Fe(1)	175.6(5)	C(80)−Fe(1)−C(60)	91.4(3)
C(30)−N(31)-Ru(1)	174.3(5)	C(40)−Fe(1)−C(50)	90.3(2)
N(81)−C(80)−Fe(1)	179.6(6)	N(1)−Ru(1)−N(11)	89.5(2)
C(30)−Fe(1)−C(40)	89.6(3)	N(31)−Ru(1)−N(11)	90.2(2)
C(30)−Fe(1)−C(60)	89.2(2)		

decomposition. This property enabled the exploration of their redox properties using cyclic voltammetry in solvents with very different characteristics (i.e., water, methanol, ethanol, and acetonitrile). In all of them, the oligonuclear species were electroactive, with voltammetric responses showing different degrees of complexity. Table 4 lists the available values that were measured for these compounds, while Figure 2 displays the typical voltammetric scans in water and acetonitrile to illustrate the solvent dependency of the redox processes.

Anodic scans starting at the open circuit potential on compounds **1**−**6** reveal quasi-reversible one-electron waves (ΔE_p in the range of 60−250 mV) which resemble the electrochemical response of the mononuclear $Ru(py)_4X_2$ and $Ru(bpy)_2X_2$ (X stands for an halide or pseudo-halide anion)[9,17] species and can therefore be ascribed to ruthenium-centered oxidation processes. The $E_{1/2}$ values are strongly dependent on the coordination environment of the Ru center and increase as the ligands become poorer σ-donors or stronger π-acceptors.

The iron centers in compounds **1**−**6** can be reduced when scanning to cathodic potentials. These processes are completely reversible on the CV time scale if measured in water (Figure 2), but for compounds **5** and **6**, they become irreversible in other solvents (even at scan rates up to 1 V s^{-1}); this is probably due to the higher lability of the $Fe^{II}(CN)_5$ moiety, particularly in organic media.[18,19] For trinuclear compounds **1**−**5**, the integrated current for full reduction accounts, as expected, for two electrons per molecule. For **6**, holding one iron center, only one electron is required for complete reduction. As it is clear from Figure 2, the appearance of the cyclic voltammetry scans is not the same for all of the trinuclear species. Two consecutive one-electron reduction processes are clearly resolved in **1a**−**3a**, with wave-to-

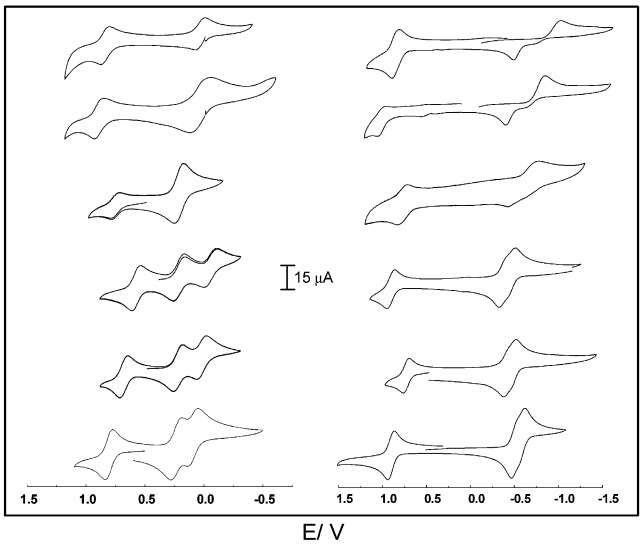

Figure 2. Cyclic voltammograms in water (left) and acetonitrile (right) of compounds **1**−**6** (bottom to top).

(17) Durham, B.; Walsh, J. L.; Carter, C. L.; Meyer, T. J. *Inorg. Chem.* **1980**, *19*, 860−865.

(18) Toma, H. E.; Takasugi, M. S. *Polyhedron* **1989**, *8*, 941.

(19) Ketterle, M.; Kaim, W.; Olabe, J. A.; Parise, A. R.; Fiedler, J. *Inorg. Chim. Acta* **1999**, *291*, 66−73.

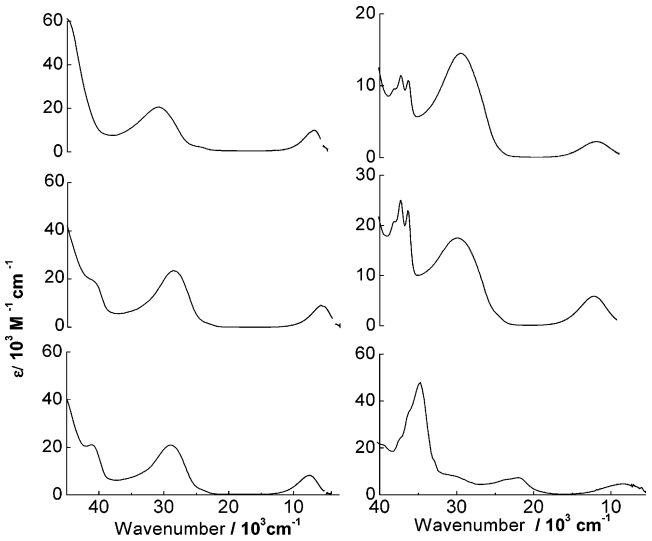

Figure 3. UV−vis−NIR spectra of **1**−**6** in water. Left, from bottom to top: **1**−**3**. Right, from bottom to top: **4**−**6**.

wave separations (ΔE_{Fe}) that increase in the order $\Delta E_{Fe}(1) < \Delta E_{Fe}(2) < \Delta E_{Fe}(3)$. These separations become significantly larger in water (140, 200, and 260 mV for **1**, **2**, and **3**, respectively), increasing the stability window for the $Fe^{II}-Ru^{II}-Fe^{III}$ species. For compounds **4** and **5**, the reduction of both hexacyanoferrate moieties seems to occur at roughly the same potential giving rise to a single and broad reduction wave, which does not resolve as individual events in any solvent.

The redox potentials of the iron-centered processes depend more strongly on the solvent properties than do those of the ruthenium-centered ones and, for any given species, span a range that can be as large as 900 mV. Figure 2 displays the changes observed in the cyclic voltammetry response upon shifting the solvent from water to acetonitrile. In all of the compounds reported here, the redox potentials for the reduction of the Fe^{III} centers correlate linearly and shift upward with the acidity of the solvent, measured by Guttman's acceptor number (Figure S1 of the Supporting Information). High acceptor solvents also induce a larger separation between the two consecutive iron-centered processes.

Electronic Spectroscopy. The species prepared in this work are strongly colored and present a rich electronic spectroscopy. Spectra measured in water on the sodium salts of the compounds are particularly valuable as they do not display the features due to the absorption bands of the PPh_4^+ counterion at 37.3×10^3 and 36.2×10^3 cm^{-1}, allowing for a better description of the spectra in the UV region. These spectra are available for compounds **1a**−**3a**, while only the PPh_4^+ was studied for compounds **4**−**6**. Figure 3 shows the results for all of the compounds in a water solution, while the most important spectroscopic features are collected in Table 4, which also contains information for other solvents.

The high-energy side of the spectra is dominated by the spectroscopic features common to the monomeric $Ru^{II}L_4X_2$ (or $Ru(bpy)_2X_2$) fragments.[9,17] For the substituted pyridine-containing compounds **1a**−**3a**, **5**, and **6**, these features include the intrapyridine $\pi \rightarrow \pi^*$ transition in the range of $(41.0-45.0) \times 10^3$ cm^{-1} and the $d_{Ru(II)} \rightarrow \pi^*_{py}$ MLCT (metal-to-ligand charge transfer) in the $(25-30) \times 10^3$ cm^{-1} region. For the bisbipyridine-based complex **4**, these features are replaced by the $\pi \rightarrow \pi^*$ transition centered on the bipyridine ligands at $\sim 35 \times 10^3$ cm^{-1} and the typical band pattern in the visible region arising from the $d_{Ru(II)} \rightarrow \pi^*_{bpy}$ CT.[9,17] The absorptions due to the $Fe^{III}(CN)_6$ [or $Fe^{III}(CN)_5X$] chromophores[20,21] are mostly obscured by the intense ruthenium-derived MLCT bands; nevertheless, the $\pi_{CN^-} \rightarrow d_{Fe(III)}$ LMCT bands are partially observed in compounds **1a**−**3a** as shoulders on the low-energy side of the MLCT bands.

The most relevant aspect of the electronic spectroscopy of these compounds is the presence of strong ($\epsilon = (2-9) \times 10^3$ M^{-1} cm^{-1}) asymmetric NIR absorptions that are absent in the separated fragments. The energies of these bands in water follow the trend **6** ≈ **5** > **4** > **1a** > **2a** > **3a**, correlating primarily with the redox potentials for the $Ru^{III/II}$ and $Fe^{III/II}$ couples (see Table 4 and Figure 4a). In contrast with the $d_{Ru(II)} \rightarrow \pi^*_{py}$ and $d_{Ru(II)} \rightarrow \pi^*_{bpy}$ CT transitions, these NIR bands are strongly solvent dependent, shifting to higher energies when the acceptor number (AN) of the solvent decreases and following a roughly linear trend with slopes of 150−165 cm^{-1}/AN (Figure S1 of the Supporting Information). Changes in the solvent properties also affect the intensity and band shape of the NIR bands. Figure 4b shows that there is a clear dependency between the transition moment and the energy for these bands. Notice that the trinuclear species **1a**−**3a** seem to share the exact same dependency, independent of the actual identity of the species. This means that the properties of these bands seem to depend solely on the energy of the transition. Remarkably, it is possible to get completely superimposable spectra for different compounds even when they were recorded in different solvents, as illustrated in Figure S2 of the Supporting Information for the case of **2a** in methanol and **3a** in ethanol.

Electronic Spectroscopy of the Reduced Species. The electronic spectra of the one- and two-electron reduced species derived from compounds **1a**−**3a** became available by chemical reduction in methanol using $S_2O_4^{2-}$ as the reducing agent. Addition of a large excess of dithionite allows the spectra of the fully reduced species of **1c**, **2c**, and **3c** (see Figure 5) to be obtained. However, the direct observation of the pure one-electron reduction products, **1b**, **2b**, and **3b**, was not possible because of the proximity between both redox processes on the iron centers. To overcome this complication, we performed a stepwise addition of $S_2O_4^{2-}$ and the spectra of **1b**, **2b**, and **3b** were recovered by mathematical treatment of the recorded data. For any addition of $S_2O_4^{2-}$, which behaves as a one-electron reducing agent, the following relations are valid:

$$[Xa] + [Xb] + [Xb] = \frac{c_0 V_0}{V + V_0}$$

$$[Xb] + 2[Xc] = \frac{cV}{V + V_0}$$

$$K_c = \frac{[Xb]^2}{[Xa][Xc]}$$

where c_0 and V_0 are the molar concentration and the volume,

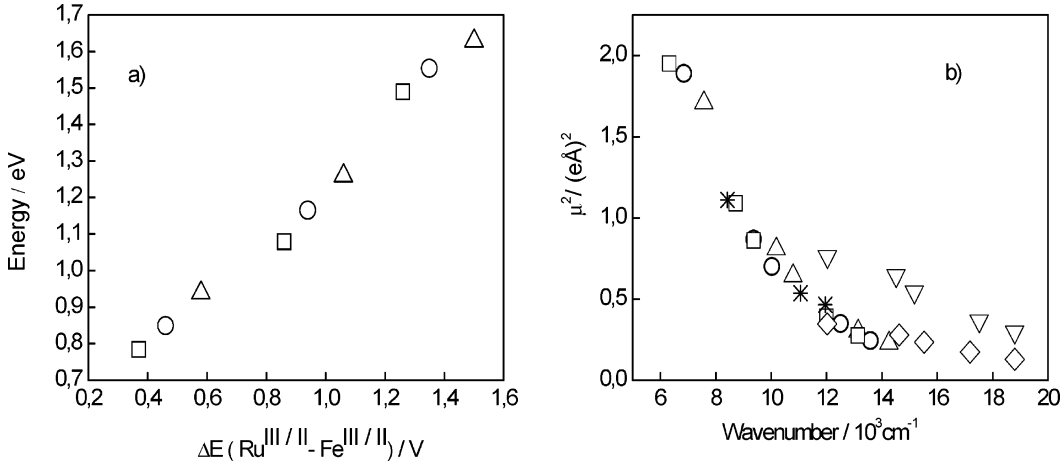

Figure 4. (a) Energy of the MMCT band for **1a** (△), **2** (○), and **3a** (□) as a function of the difference of redox potentials of the $Ru^{III/II}$ and $Fe^{III/II}$ couples. (b) Transition moment of the MMCT transition as a function of its energy: **1a** (△), **2a** (○), **3a** (□), **4** (∗), and **5** (▽).

Table 4. UV−vis−NIR and Electrochemical Properties of Compounds **1**−**6** in Different Solvents

		$\bar{\nu}_{max}$, $\times 10^3$ cm^{-1} (ϵ, $\times 10^3$ M^{-1} cm^{-1}) [$\Delta\bar{\nu}_{1/2}$, $\times 10^3$ cm^{-1}]		$E_{1/2}$, V (ΔE_p, mV)[a]		
complex	solvent	MLCT	MMCT	$Ru^{III/II}$	$Fe^{III/II}$	
1	water	29.1 (27.5)	7.6 (8.1) [3.8]	0.81 (70)	0.23 (90)	0.095 (80)
	methanol	27.9 (22.3)	10.2 (4.9) [3.8]	0.87 (80)	−0.19 (70)	−0.31 (70)
	ethanol	27.3 (22.4)	10.8 (4.2) [4.3]	0.83 (150)	−0.22 (130)	−0.33 (100)
	acetonitrile	26.8 (21.7)	13.1 (2.5) [3.7]	0.90 (70)	−0.60 (60)	−0.69 (50)
	dimethylacetamide	25.8 (25.8)	14.3 (2.2) [3.5]			
1b[b]	methanol	26.5 (24.3)	7.8 (3.4) [3.8]			
1c[b]	methanol	25.7 (25.7)				
2	water	29.0 (26.6)	6.9 (8.9) [3.3]	0.69 (70)	0.23 (80)	0.032 (84)
	methanol	27.8 (24.8)	9.4 (5.4) [3.5]	0.79 (100)	−0.15 (116)	−0.29 (120)
	ethanol	27.1 (24.7)	10.1 (4.8) [3.7]	0.71 (210)	−0.29 (256)	−0.56 (260)
	acetonitrile	26.6 (26.6)	12.5 (2.9) [3.7]	0.73 (70)	−0.62 (50)	−0.73 (60)
	dimethylacetamide	25.5 (28.2)	13.7 (2.3) [3.7]			
2b[b]	methanol	26.6 (27.6)	7.2 (4.0) [3.8]			
2c[b]	methanol	25.6 (29.3)				
3	water	30.1 (22.4)	6.3 (9.9) [3.1]	0.59 (80)	0.22 (100)	−0.044 (112)
	methanol	29.6 (20.9)	8.7 (5.9) [3.6]	0.653 (80)	−0.212 (80)	−0.382 (90)
	ethanol	29.1 (20.5)	9.4 (5.1) [3.7]	0.61 (210)	−0.46 (220)	−0.66 (210)
	acetonitrile	28.1 (19.6)	12.0 (2.9) [3.7]	0.63 (90)	−0.63 (70)	−0.73 (70)
	dimethylacetamide	26.8 (21.9)	13.1 (2.5) [3.9]			
3b[b]	methanol	28.3 (21.4)	6.5 (4.6) [4.4]			
3c[b]	methanol	26.7 (22.4)				
4	water	22.0 (7.3)	8.4 (4.6) [5.8]	0.77 (71)	0.23 (81)	
	methanol	20.7 (9.2)	11.1 (3.6) [5.0]			
	ethanol	20.6 (9.5)	12.0 (3.0) [4.8]			
	acetonitrile	20.1 (9.5)	14.4 sh (2.3)	0.77 (112)	−0.99 (400)	
	dimethylacetamide	19.4 (11.1)	15.2 sh (2.8)			
5	water	29.9 (17.5)	12.0 (5.9) [4.2]	0.91 (80)	0.044 (79)	
	methanol	28.5 (17.7)	14.5 (5.4) [4.1]	1.04 (80)	−0.35 (240)[c]	
	ethanol	27.9 (17.8)	15.2 (5.2) [3.7]	1.06 (250)	−0.56 (330)[c]	
	acetonitrile	27.8 (17.8)	17.5 (4.2) [3.6]	1.01 (80)	−0.86 (400)[c]	
	dimethylacetamide	25.8 (20.1)	18.8 (3.8) [3.4]			
6	water	29.6 (14.5)	12.0 (2.2 [4.2]	0.85 (80)	0.044 (82)	
	methanol	28.4 (18.3)	14.6 (2.3) [3.9]	1.01 (70)	−0.31 (260)[c]	
	ethanol	29.0 (18.6)	15.6 (2.2) [3.9]	1.04 (200)	−0.52 (170)[c]	
	acetonitrile	27.3 (19.7)	17.2 (2.0) [3.7]	0.85 (80)	−0.98 (280)[c]	
	dimethylacetamide	26.0 (20.1)	18.8 (1.6) [3.5]			

[a] Against Ag/AgCl, 3 M KCl. [b] See text for details of the deconvolution of the spectra of these species. [c] Irreversible wave.

respectively, of the solution of the initial compounds **1a**, **2a**, and **3a**, and c and V are the concentration and the added volume, respectively, of $S_2O_4^{2-}$. The brackets denote molar concentrations, and K_c is the comproportionation constant defined for the following process:

$$[Xa] + [Xc] \overset{K_c}{\rightleftharpoons} [Xb] \qquad K_c = e^{F\Delta E/(RT)}$$

This constant is related to the difference in redox potentials for the two $Fe^{III/II}$ couples (ΔE) measured in the cyclic voltammetry experiments and in methanol takes the values of 1.1 $\times 10^2$, 2.3 $\times 10^2$, and 7.5 $\times 10^2$ for **1**, **2**, and **3**, respectively.

The concentration of all of the species present in solution can be obtained by solving the system of equations, and mathematical deconvolution of the spectra for the mixtures,

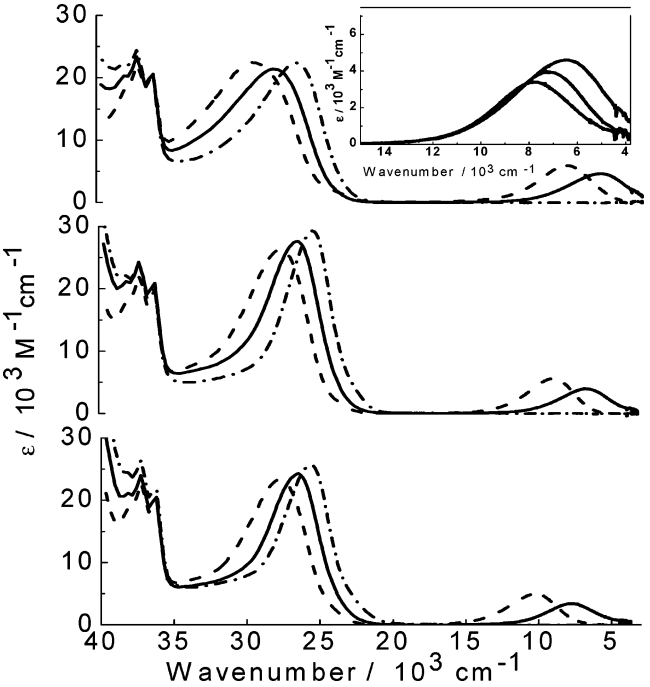

Figure 5. UV−vis−NIR spectra of **1**−**3** (top to bottom) in methanol for the three oxidation states: $Fe^{III}-Ru^{II}-Fe^{III}$ (- - -), $Fe^{II}-Ru^{II}-Fe^{III}$ (—), and $Fe^{II}-Ru^{II}-Fe^{II}$ (- · -). Inset: overlayed NIR spectra of **1b**, **2b**, and **3b**.

provided that the ones for the pure **1a**−**3a** and **1c**−**3c** are known, yields the spectra for **1b**−**3b**.

As observed in Figure 5, the vis−NIR spectra of these latter species contain essentially the same features as described for **1a**−**3a**. The $d_{Ru(II)} \rightarrow \pi^*_{py}$ bands can still be observed at 26.6×10^3, 26.7×10^3, and 28.2×10^3 cm^{-1} for **1b**, **2b**, and **3b**, respectively. NIR absorptions are also present but with a lower intensity than in **1a**−**3a** (Table 4). As observed with the MLCT bands, they are displaced to a lower energy ($\sim(2-5) \times 10^3$ cm^{-1}). The NIR absorption in **1b** is symmetrical and roughly Gaussian shaped, but a shoulder at a higher energy is noticed in **2b** and seen more clearly in **3b**. In the fully reduced species, the NIR bands vanish completely, and the only intense absorptions remaining are the $d_{Ru(II)} \rightarrow \pi^*_{py}$ at even lower energies than those in **1b**, **2b**, and **3b**.

Discussion

The preparation of the trinuclear complexes described in this work involved either the simultaneous substitution of two chloride ions by $[Fe(CN)_6]^{3-}$ in the readily available *trans*-RuL_4Cl_2 (or *cis*-$Ru(bpy)_2Cl_2$) species or the reaction of the more labile $[Fe(CN)_5NH_3]^{3-}$ compound[20,21] with the inert fragment *trans*-$RuL_4(CN)_2$. In all of the cases, the structural and spectroscopic evidence suggest that the reactions proceed with retention of the conformation on the ruthenium center, yielding analytically pure species.

For many years, the number of structurally well-characterized linear cyano-bridged heterotrinuclear species remained scarce, with *trans*-$[(NH_3)_4Pt^{IV}\{NC-Fe^{II}(CN)_5\}_2]^{4-}$ as the most remarkable example.[7] Only recently, a substantial number of trinuclear cyano-bridged compounds became available.[5,6] Among them, those based on the $M(py)_4$ core and general formula *trans*-$[M(py)_4\{NC-M'(CO)_5\}_2]$ ($M = Mn^{2+}$, Co^{2+}, or Ni^{2+}; $M' =$ Mo, W)[22] are closely related to the ones reported here and therefore are useful for comparison purposes. Although the latter compounds have different metal centers than the ones synthesized in this work and also lack terminal cyanide molecules, some structural similarities with **1a** and **2a** are striking. These trinuclear species display virtually octahedral coordination environments around the metal centers, almost linear arrangements of the three metal ions, and an almost perfectly eclipsed disposition of the equatorial ligands. This last observation is at least curious. This type of configuration was also observed in the homonuclear *trans*-$[py_4Ru^{II}\{NC-Ru^{II}py_4Cl\}_2]^{2+}$ cation[16] but not in the related *trans*-$[(NH3)_4Pt^{IV}\{NC-Fe^{II}(CN)_5\}_2]^{4-}$ anion,[7] where the ligands in the equatorial positions are staggered. Arguments, purely based on steric factors, would actually favor this last configuration. It has been argued[16] that in the eclipsed conformation, the d_{xz} and d_{yz} orbitals of the three metals overlap the π orbitals of the bridging cyanides. For this reason, the preference for this particular configuration has been taken as an indication of metal−metal interaction along an extended backbone involving orbitals of π symmetry. Though tempting, this line of reasoning has to be employed carefully. In our case, and also with the *trans*-$[M(py)_4\{NC-M'(CO)_5\}_2]$ species described in ref 22, the steric requirements imposed by the ligand environment of the terminal metallofragments are certainly less constraining than in the *trans*-$[py_4Ru^{II}\{NC-Ru^{II}py_4Cl\}_2]^{2+}$ species, and therefore the observed configuration might not necessarily be indicative of strong electronic coupling between the fragments.

The pyridines in compound **1a** adopt the usual propeller-like configuration observed in many $M(py)_4X_2$ compounds, particularly in those containing ruthenium.[9] This characteristic is also shared with the previously mentioned *trans*-$[py_4Ru^{II}\{NC-Ru^{II}py_4Cl\}_2]^{2+}$ and *trans*-$[M(py)_4\{NC-M'(CO)_5\}_2]$ species but not with **2a**. For the latter, the pyridine rings are also tilted but with alternating orientations (Figure 1). It is not clear whether the differences are due to electronic or packing effects.

The most reliable structural evidence of measurable $d\pi(Ru^{II}) \rightarrow \pi^*(NC)$ back-bonding interactions, though not conclusive, arises from the short Ru−N(nitrile) bond lengths (2.017 Å for **1a** and 2.012 Å for **2a**), which are very similar to the reported value for $[py_4Ru^{II}\{NC-Ru^{II}py_4Cl\}_2]^{2+}$ (Ru−N bond distance = 2.013 Å) and shorter than the usual bond lengths reported in other cyanide-bridged complexes.[5,23] Better arguments in favor of extended electronic interactions among the metal centers show up not from solid-state studies but from experiments in solution.

(20) Macartney, D. H. *Rev. Inorg. Chem.* **1988**, *9*, 101.
(21) Baraldo, L. M.; Forlano, P.; Parise, A. R.; Slep, L. D.; Olabe, J. A. *Coord. Chem. Rev.* **2001**, *219*, 881−921.
(22) Vahrenkamp, H.; Sheng, T. *Inorg. Chim. Acta* **2004**, *357*, 1739.
(23) (a) Christofides, A.; Connelly, N. G.; Lawson, H. J.; Loyns, A. C.; Orpen, A. G.; Simmonds, M. O.; Worth, G. H. *J. Chem. Soc., Dalton Trans.* **1991**, 1595−1601. (b) Bignozzi, C. A.; Chiorboli, C.; Indelli, M. T.; Scandola, F.; Bertolasi, V.; Gilli, G. *J. Chem. Soc., Dalton Trans.* **1994**, 2391−2395.

The new species described here, in contrast with the *trans*-$[M(py)_4\{NC\text{-}M'(CO)_5\}_2]$ counterparts, proved to be quite robust, principally, because of the increased inertness of the Ru(II) center compared to the first-row metal ions employed in the previously mentioned series. This enabled the use of a whole set of experimental techniques not available for labile species. The use of cyclic voltammetry revealed that the metal centers in compounds **1**−**6** could engage in consecutive one-electron transfer processes, without any significant change in the stability of the compounds.

Compounds **1**−**4** result from the replacement of two chloride ions by hexacyanoferrate(III) in the monomeric $Ru(py)_4Cl_2$ or $Ru(bpy)_2Cl_2$ precursors. This change induces a shift of the $Ru^{III/II}$ couples of approximately 500−600 mV to higher potentials, probably because of the smaller σ-donor and higher π-acceptor capabilities of the $[Fe(CN)_6]^{3-}$ fragment compared to that of a chloride ion. To our knowledge, there are no well-reported examples in the literature of electrochemical behavior of ruthenium centers holding a $[Fe^{III}(CN)_6]^{3-}$ moiety because the most common examples involve electron-rich Ru centers, which oxidize at lower potentials than those of the $Fe^{III/II}$ couple. These four cases provide an estimate of the Lever parameter[24] for a ferricyanide ligand (an average of 250−300 mV), a value that could be worthwhile for assisting in the prediction of the redox properties of unknown compounds.

The cyclic voltammetry exploration of the redox behavior of anion **5** revealed that the $Ru^{III/II}$ couple is only slightly shifted to higher potentials compared to the one in $Ru(py)_4(CN)_2$. This contrasts with the results observed for other trinuclear complexes using the same fragment as a bridge, where the $Ru^{III/II}$ redox potential shows a large increase upon metalation of the exposed cyanide.[16,25] These trends seem to be offset here by the negative charge of the $[Fe^{III}(CN)_5]^{3-}$ fragment that contrasts with the cationic nature of the terminal fragments in all of the other reported examples. Anion **6** shows an even smaller shift due to the presence of only one terminal ferricyanide fragment.

Remarkably, there seems to be little influence of the solvent on the redox properties of the $Ru^{III/II}$ couples. On the contrary, the redox potentials of the $Fe^{III/II}$ couples of complexes **1**−**6** have a significant solvent dependency, with a roughly linear correlation between the $Fe^{III/II}$ redox potential and Guttman's acceptor number,[26] regardless of the number of observed $Fe^{III/II}$ waves (Figure S1 of the Supporting Information).

This type of dependency has been previously observed in other cyanide-containing compounds[21,27] and explained in terms of a simple donor−acceptor model. It is generally accepted that the terminal cyanides and the solvent molecules are involved in donor−acceptor (or acid−base) interactions that make the cyanides increasingly better π acceptors toward the metal center as the acceptor properties of the solvent increase. This interaction enhances the iron-to-cyanide backbonding, stabilizing the Fe^{II} state and therefore increasing the redox potential of the $Fe^{III/II}$ couples. The observed slopes for the $E_{1/2}$ (in millivolts) versus AN plots are virtually the same for all of the compounds described here, ranging between 22 and 29 mV/AN (Figure S1 of the Supporting Information). It has been suggested that these figures should depend solely on the number of terminal cyanides coordinated to the redox center and exposed to the solvent,[27] and actually, our results for complexes **1**−**6**, though slightly larger, are comparable to those arising from other fragments containing five terminal cyanides [19 ± 5 for $[Ru^{II}(CN)_5Mepz]^{2-}$ [27] and 17 ± 1 for $[Os^{II}(CN)_5pz]^{3-}$).[28]

Perhaps the most impressive consequence of changing the solvent resides on the splitting of the redox processes on the Fe centers in a way that resembles previous reports on the pyrazine-bridged di-iron compound $[(NC)_5Fe\text{-}pz\text{-}Fe(CN)_5]^{n-}$.[19] Particularly, the observed ΔE_{Fe} values for complexes **1a**−**3a** decrease when going from water to acetonitrile from 140, 200, and 260 mV to 90, 110, and 100 mV for **1a**, **2a**, and **3a**, respectively. It is well established that the magnitude of the splitting between the two consecutive redox processes on the terminal fragments, or equivalently the size of the comproportionation constant K_c, can be taken as a measurement of the efficiency of the electronic coupling between redox active centers. For **1a**−**3a**, K_c in water becomes $10^{2.4}$, $10^{3.4}$, and $10^{4.4}$, respectively, but lowers significantly to $10^{1.5}$, $10^{1.9}$, and $10^{1.7}$ for the same compounds in acetonitrile. The whole set of values is still perfectly comparable to those reported in other class II mixed-valent di-iron species, which means that these molecules behave as electronically coupled dinuclear iron complexes bridged by a redox active $-CN-Ru^{II}L_4-NC-$ unit that provides a path for the electronic interaction between the terminal fragments. As is clear from the numbers discussed above and those from Table 4, the electronic communication between the Fe centers seems to be influenced by the nature of the substituents on the pyridine rings. Electron-donating groups lower the potential for the $Ru^{III/II}$ couple located in the bridge unit and increase ΔE_{Fe}, suggesting that the electronic coupling between the terminal irons involves high-lying filled d_π orbitals on the bridge (hole-transfer mechanism), in contrast to the above-mentioned $[(NC)_5Fe\text{-}pz\text{-}Fe(CN)_5]^{n-}$ ion.[19] For the latter, as with other pyrazine-bridged dinuclear species, low-lying empty π^* orbitals on the bridge provide the pathway for electron tranfer between the metal centers.[29]

(24) Lever, A. B. P. *Inorg. Chem.* **1990**, *29*, 1271−1285.
(25) Macatangay, A. V.; Endicott, J. F. *Inorg. Chem.* **2000**, *39*, 437−446.
(26) Gutmann, V. *Electrochim. Acta* **1976**, *21*, 661−670.
(27) Timpson, C. J.; Bignozzi, C. A.; Sullivan, B. P.; Kober, E. M.; Meyer, T. J. *J. Phys. Chem.* **1996**, *100*, 2915−2925.
(28) Slep, L. D.; Baraldo, L. M.; Olabe, J. A. *Inorg. Chem.* **1996**, *35*, 6327−6333.
(29) (a) Furholz, U.; Burgi, H. B.; Wagner, F. E.; Stebler, A.; Ammeter, J. H.; Krausz, E.; Clark, R. J. H.; Stead, M. J.; Ludi, A. *J. Am. Chem. Soc.* **1984**, *106*, 121−123. (b) Zhang, L. T.; Ko, J.; Ondrechen, M. J. *J. Am. Chem. Soc.* **1987**, *109*, 1666−1671. (c) Ferretti, A.; Lami, A. *Chem. Phys. Lett.* **1994**, *220*, 327−330. (d) Zhang, L. T.; Ondrechen, M. J. *Inorg. Chim. Acta* **1994**, *226*, 43−51. (e) Hornung, F. M.; Baumann, F.; Kaim, W.; Olabe, J. A.; Slep, L. D.; Fiedler, J. *Inorg. Chem.* **1998**, *37*, 311−316. (f) Ferretti, A.; Lami, A.; Murga, L. F.; Shehadi, I. A.; Ondrechen, M. J.; Villani, G. *J. Am. Chem. Soc.* **1999**, *121*, 2594−2596. (g) Scheiring, T.; Kaim, W.; Olabe, J. A.; Parise, A. R.; Fiedler, J. *Inorg. Chim. Acta* **2000**, *300*, 125−130. (h) Kaim, W.; Klein, A.; Glockle, M. *Acc. Chem. Res.* **2000**, *33*, 755−763.

This simplified picture provides most of the tools that are needed to analyze the amount of electronic delocalization in these three linear molecules and can be easily extended to compound **5**. Exploration of its cyclic voltammetry reveals only one wave for the terminal irons. This behavior could be ascribed to the larger difference in redox potential between the bridge and the terminal moieties. The lack of an energy match induces a poor orbital mixing between the Ru and Fe centers that results in a highly reduced degree of electronic delocalization through the bridge, as suggested by the lack of splitting of the iron-centered redox couples.

Notice however that the energy of the d_π orbitals in the bridging fragment is not the only factor to take into account. In fact, geometric aspects also have a marked influence in modulating the interaction between the orbitals of the terminal metals. Consider, for example, compounds **1** and **4**: both have the same terminal hexacyanoferrate fragments, almost identical redox properties of the bridge, but a different geometry. This single change, far from being minor, has a large impact on the cyclic voltammetry response that shows no resolution for the Fe-centered events. A similar behavior has been observed for other trinuclear species holding a Pt(II) as the central ion, where the redox processes on the terminal fragments are differentiated for the trans but not for the cis configuration.[5b,c] These results support the idea that linear arrangements might be more suited to promote a high degree of electronic delocalization between distant fragments, though more studies have to be carried out in order to establish the generality of this statement.

The high stability of the species described in this report additionally enabled a complete characterization of their electronic spectroscopy. This holds not only for the parent compounds but also for the one- and two-electron reduced species, **1b**−**3b** and **1c**−**3c**. These types of studies provided a deeper insight into the communicating properties of the different fragments.

All of the solids isolated in this report are intensely colored mainly because of the presence of a low-energy asymmetric absorption band, which is absent in any of their constituting moieties. These bands vanish completely upon full reduction of the molecules, suggesting that they arise from the mixed-valent nature of these species. Compounds **1**−**5** are examples of mixed-valent heterodinuclear compounds with Ru^{II} and Fe^{III} metal ions linked by a bridging fragment with π orbitals of the appropriate symmetry interacting with the t_{2g} sets on the metal centers. This arrangement of species with d^5 and d^6 electronic configurations is probably responsible for the observed metal-to-metal charge transfer (MMCT) bands. The assignment of the bands as $Ru^{II} \rightarrow Fe^{III}$ CT is supported by the experimental correlation between the energy of the bands and the redox properties of the metal centers (Figure 4a).

The existence of these transitions enables a spectroscopic evaluation of the electronic delocalization between the donor Ru^{II} and the acceptor Fe^{III} fragments mediated by the π system of the bridging cyanide. This problem has been classically studied in binuclear systems, where an estimation of the electronic coupling was achieved by employing the Born−Oppenheimer approximation and first-order perturbation theory arguments (Marcus−Hush formalism). The donor−acceptor interaction has been described in terms of H_{DA}, the off-diagonal electronic-coupling matrix element, which can be estimated from the experimental oscillator strength and full width at half-height of the absorption band. This formalism is more than 35 years old,[30] but in the 1990s, the field has experienced a renaissance as a consequence of the synthesis and characterization of novel donor−acceptor systems.[31,32] One of the most successful treatments derived from the original Marcus−Hush formalism involves the use of a two-state model and its extension to more complex systems involving three or four states.[31,32] We follow these lines, at least qualitatively, to provide a better spectral assignment and analyze our experimental findings on the MMCT bands of these compounds.

In the absence of electronic coupling between the metal centers, our trinuclear systems containing two Fe^{III} fragments and a Ru^{II} center can adopt one of three possible "diabatic" states,[31,32] described as (1) $Fe^{III}-Ru^{II}-Fe^{III}$, (2) $Fe^{II}-Ru^{III}-Fe^{III}$, and (3) $Fe^{III}-Ru^{III}-Fe^{II}$, with (1) being lower in energy (ground state) and (2) and (3) lying at an energy E above the ground state (Figure 6a). The electronic coupling between neighbor fragments is introduced in this description by means of the off-diagonal matrix elements, $H_{12} = H_{13}$, that induce mixing of these states to produce three "adiabatic" free-energy surfaces (Figure 6a).[33] Two CT bands between the adiabatic states are expected within this description. One of them is strictly forbidden at the equilibrium geometry though activated by vibronic coupling with antisymmetric modes. These two bands are not resolved in our compounds, but their presence can be inferred from the asymmetric profile of the MMCT bands that results in a marked tail on the high-energy side.

This simple picture allows one to understand most of the experimental findings. In the ground state, the iron centers are better described as Fe^{III}, with some Fe^{II} characteristics arising from the electronic interaction with the Ru^{II} center. On the contrary, in any of the excited states that follow the CT process, these iron centers have a large degree of Fe^{II} characteristics. This results in a better specific interaction of the terminal cyanides with molecules of the solvent, which results in a decrease of the CT energies in acceptor solvents.

We also observed that this behavior coincides with the changes in the transition moment. Unlike the original Marcus−Hush formalism, the integrated absorption intensity of the MMCT bands in these three-state systems cannot be related by a simple equation to the amount of electronic delocalization, requiring extensive modeling to achieve

(30) (a) Hush, N. S. *Prog. Inorg. Chem.* **1967**, *8*, 391−444. (b) Hush, N. S. *Electrochim. Acta* **1968**, *13*, 1005−1023.
(31) (a) Creutz, C.; Newton, M. D.; Sutin, N. *J. Photochem. Photobiol., A* **1994**, *82*, 47−59. (b) Brunschwig, B. S.; Creutz, C.; Sutin, N. *Coord. Chem. Rev.* **1998**, *177*, 61−79. (c) Brunschwig, B. S.; Creutz, C.; Sutin, N. *Chem. Soc. Rev.* **2002**, *31*, 168−184.
(32) (a) Lambert, C.; Noll, G. *J. Am. Chem. Soc.* **1999**, *121*, 8434−8442. (b) Lambert, C.; Noll, G. *J. Chem. Soc., Perkin Trans. 2* **2002**, 2039−2043. (c) Lambert, C.; Noll, G.; Schelter, J. *Nat. Mater.* **2002**, *1*, 69−73.
(33) The matrix elements, H_{23} and H_{32}, can be safely assumed to be negligible, provided there is large separation between the terminal metal centers.

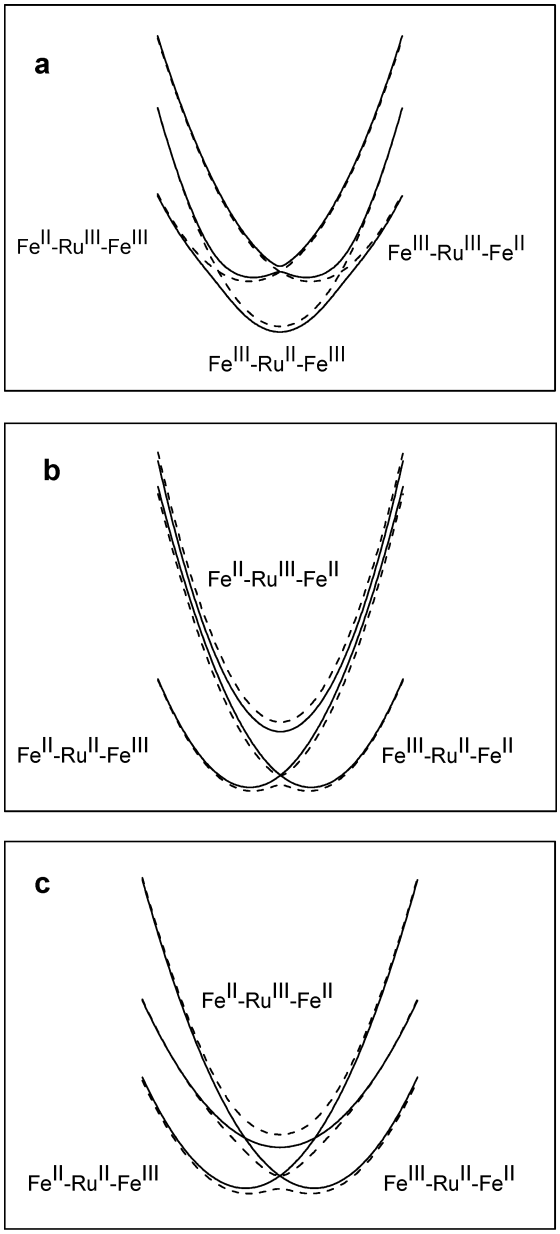

Figure 6. Plots of qualitative potential energy surfaces, including the diabatic states (full line) and the adiabatic states (dashed line) for the $Fe^{III}-Ru^{II}-Fe^{III}$ system (a), and two different energy arrangements for the $Fe^{II}-Ru^{II}-Fe^{III}$ system (b and c).

quantitative information. Nevertheless, a qualitative treatment of the problem still produces valuable information about the extent of electronic coupling between the centers. The oscillator strength of the MMCT is still diagnostic of the extent of electronic delocalization, and the intensity of these bands is expected to increase with increasing electronic coupling. A plot of the transition moment against the energy of the CT band for this family of molecules in different solvents (Figure 4b) shows a marked increase in the intensity of the MMCT bands associated with a decrease in their energy, as expected. On the basis of the spectroscopic information, the higher degree of electronic coupling is achieved in water. In this solvent, and on the basis of the intensity of the MMCT band, the extent of electronic delocalization between the Fe^{III} and Ru^{II} centers seems to increase in the order **1a** < **2a** < **3a**. It is remarkable that the data arising from many solvents for the three structurally related **1a**−**3a** could be arranged on the same μ versus E_{CT} curve, and even more impressive is the strong similarity between the spectral shapes. These facts suggest that the free-energy surfaces for the diabatic states are independent of the equatorial ligands on the Ru^{II} and are not related to the solvent properties. When any of these two factors are changed, the energy of the diabatic states seems to finely modulate, but the shape of these surfaces is not affected.

The relatively large separation between the two reduction waves in compounds **1**−**3** in solvents with high AN allowed us to chemically reduce these species. The preference for methanol instead of water to perform these experiments enabled the collection of information in a spectral window ranging from 200 to ∼3000 nm. This selection, however, forced the use of mathematical tools for spectral deconvolution for overcoming the insufficient separation of the reduction potentials of the iron fragments. The one- and two-electron reduced species proved to be extremely stable in methanolic solution, except for their high reactivity against molecular oxygen.

One-electron reduction of compounds **1a**−**3a** to yield **1b**−**3b** induces shifts of the $d_{Ru(II)} \rightarrow \pi^*_L$ MLCT transitions to lower energies, as expected from replacing one terminal ferricyanide moiety by the better σ-donor Fe^{II} analogue. The energies and intensities of the MMCT bands are even more affected by the reduction event, as observed in Figure 5.

Species **1b**−**3b** are better visualized as mixed-valent di-iron compounds, bridged by a nontypical $-CN-Ru^{II}L_4-NC-$ electron donor fragment. This situation was described long ago for $[(NH_3)_5RuImRu(NH_3)_5]^{4+}$ (Im^- = imidazolate),[34] a molecule that displays an intense MMCT band in the visible region of the spectrum. More recently, a series of reports on other molecules bridged by π-donor fragments, including binuclear complexes,[35] trinuclear complexes,[6,25] and metal-free mixed-valent species,[32,36] have appeared in the literature.

The electronic spectroscopy of some of these species has also been treated by means of a three-state model, which locates the extra electron on any of the three fragments involved. Electronic interactions between the neighbor fragments are responsible for the electronic delocalization along the entire molecule. For these $M^{II}-B-M^{III}$ systems, the three relevant diabatic states required for the description of the electronic spectroscopy are the degenerate $M^{II}-B-M^{III}$, $M^{III}-B-M^{II}$, and one higher lying state accounting for a net transfer of one electron from the bridge to the terminal fragments ($M^{II}-B^+-M^{II}$). Electronic coupling leads to the three adiabatic potential energy surfaces qualitatively depicted in Figure 6b, which successfully explained the

(34) Isied, S. S.; Kuehn, C. G. *J. Am. Chem. Soc.* **1978**, *100*, 6754−6756.
(35) (a) Rezvani, A. R.; Evans, C. E. B.; Crutchley, R. J. *Inorg. Chem.* **1995**, *34*, 4600−4604. (b) Rezvani, A. R.; Bensimon, C.; Cromp, B.; Reber, C.; Greedan, J. E.; Kondratiev, V. V.; Crutchley, R. J. *Inorg. Chem.* **1997**, *36*, 3322−3329. (c) Evans, C. E. B.; Yap, G. P. A.; Crutchley, R. J. *Inorg. Chem.* **1998**, *37*, 6161−6167.
(36) Lambert, C.; Noll, G. *Angew. Chem., Int. Ed.* **1998**, *37*, 2107−2110.

occurrence of two CT absorptions in many compounds with the characteristics mentioned above. The usually more intense transition at a higher energy corresponds roughly to a CT involving the bridge orbitals of π symmetry and a hole in the d_π set of the terminal moieties (or alternatively a half-occupied π orbital for the full organic systems). The second one, red-shifted and weaker, involves the mixed-valent distant fragments coupled through the bridge.

Compounds **1b**−**3b** display, however, only one intense band in the NIR region of the spectrum with a tail to higher energies, particularly noticeable for **2b** and **3b**. The band maxima shift to lower energies and increase in intensity when the bridging fragment becomes a better electron donor (Figure 5). The high-energy sides of the three bands, on the contrary, are almost superimposable (Figure 5). This suggests the presence of two overlapping unresolved bands: a strong one on the low-energy side of the absorption profile, whose energy depends on the identity of the bridge, and a much weaker blue-shifted one that remains unaffected in the three compounds. The different substituents on the bridge modify the energy of the low-energy component in a way that resembles the observations in the NIR bands in compounds **1a**−**3a**. We presently suggest that this low energy, but more intense, transition is better ascribed to an excited state that involves CT from the $-CN-Ru^{II}L_4-NC-$ donor fragment to the terminal Fe(III) moiety. To account for this observation, the potential energy surfaces have to be changed, as seen in Figure 6c. The better energy match between the diabatic $Fe^{II}-Ru^{II}-Fe^{III}$ and $Fe^{II}-Ru^{III}-Fe^{II}$ states should improve the electronic coupling between the Ru(II) and Fe(III) centers, explaining the high experimental transition moments that remain comparable to the observed ones in compounds **1a**−**3a**, even when only one Fe(III) center is involved.

The weak band at a higher energy does not depend on the identity of the bridge, suggesting that the excited state involved has a slight Ru(III) characteristic. This is actually the situation for the higher energy adiabatic state depicted in Figure 6c, which at the equilibrium geometry of the ground state, has negligible $Fe^{II}-Ru^{III}-Fe^{II}$ characteristics. Therefore, the high-energy component can be associated with the intervalence CT transition between the two distant iron centers. For moderate electronic coupling, as seen in Figure 6c, the reorganization energies of the $Fe^{II}-Ru^{II}-Fe^{III}$ and $Fe^{III}-Ru^{II}-Fe^{II}$ states determine the energy of this transition. In our case, this variable seems to be roughly constant along the **1b**−**3b** series, resulting in the observed insensitivity of the high-energy component to changes in the $-CN-Ru^{II}L_4-NC-$ donor fragment.

Conclusions

The complexes described in this paper contribute to the growing reports on the properties of trinuclear systems. We showed electrochemical and spectroscopic evidence that suggests that compounds **1**−**3** exhibit long-range interactions between the terminal iron fragments. The absence of this phenomenon in **4** provides more evidence that the trans configuration around the central ion promotes a better coupling between the terminal fragments in a trinuclear system.

Our results show that the electronic coupling can be tuned by changes in the solvent or the coordination sphere around the bridging fragment. Remarkably, the properties of this family of complexes follow a well-defined pattern, making it possible to anticipate over a wide range the properties of any given member of the family with great accuracy.

The large splitting between the reduction potentials for the $Fe^{III/II}$ couples in some of the compounds allowed for a spectroscopic characterization of the $Fe^{II}-Ru^{II}-Fe^{III}$ redox state. The results revealed the presence of two transitions that were very close in energy. Their behavior upon substitution on the pyridine ring suggests that the intervalence CT state [Fe(II) → Fe(III)] actually resides at a higher energy than the CT state from the bridge to the terminal iron [Ru(II) → Fe(III)].

Complexes **1**−**3** are attractive as building blocks for larger and more complex structures. They can be prepared in a multigram scale, and the presence of terminal cyanides provides a suitable linker to integrate them into larger molecules. A linear configuration for the polymerization of these trinuclear fragments should be strongly favored due to the presence of the bulky pyridines on the ruthenium coordination sphere and the tendency of these species to adopt an eclipsed configuration. All of these properties make this system a good candidate for the design of molecular wires, with tunable properties along the wire. We are actively exploring this idea.

Acknowledgment. We thank the Fundación Antorchas and the Agencia para la Promoción de la Ciencia y la Tecnología (ANPCYT) for financial support. We are also thankful to Johnson Matthey for a generous loan of precious metals and to Professor K. Wieghardt (Max-Planck-Institut für Bioanorganische Chemie) for providing access to his laboratory equipment. L.D.S. and L.M.B. are members of the scientific staff of CONICET. P.A. is a graduate fellow from the Universidad de Buenos Aires.

Supporting Information Available: Figures S1 and S2 in pdf format and crystallographic data in CIF format. This material is available free of charge via the Internet at http://pubs.acs.org.

IC0493649